Available online at www.sciencedirect.com
ScienceDirect
Acta Materialia 57 (2009) 267–277
Acta MATERIALIA
www.elsevier.com/locate/actamat

Fabrication, characterization and microwave properties of polyurethane nanocomposites reinforced with iron oxide and barium titanate nanoparticles

Z. Guo [a,*], S.-E. Lee [a], H. Kim [a], S. Park [a], H.T. Hahn [a], A.B. Karki [b], D.P. Young [b]

[a] Mechanical & Aerospace Engineering and Materials Science & Engineering Department, University of California-Los Angeles, Los Angeles, CA 90095, USA
[b] Department of Physics and Astronomy, Louisiana State University, Baton Rouge, LA 70803, USA

Received 18 June 2008; received in revised form 26 August 2008; accepted 1 September 2008
Available online 14 October 2008

Abstract

Polyurethane (PU) nanocomposites reinforced with magnetic iron oxide nanoparticles and/or dielectric barium titanate nanoparticles fabricated by the surface-initiated-polymerization approach were investigated. The polymer matrix incorporated with different nanoparticles shows different presenting status surrounding the nanoparticles, i.e., chemical bonding, physical entanglement and bulk polymer chain. The nanoparticles have a different effect on the thermal stability of the polymer nanocomposites. By embedding different functional nanoparticles, unique physical properties were observed, such as enlarged coercivity and larger dielectric constant (real permittivity). The synergistic effect of the binary nanoparticle reinforced PU nanocomposite was explored. The addition of the iron oxide nanoparticles does have some effect on the permittivity. However, little difference was observed in the magnetic properties and permeability after the introduction of the dielectric barium titanate nanoparticle into Fe_2O_3/PU nanocomposites. The permeability and permittivity of γ-Fe_2O_3 and $BaTiO_3$ nanoparticle reinforced PU nanocomposites were investigated with frequencies ranging from 10 MHz to 1 GHz. The predicted microwave properties from Bruggeman's equation were consistent with the measured data, except for the real permittivity of Fe_2O_3/$BaTiO_3$/PU. The volume average method (VAM) usually used for fiber-reinforced composites with reinforcements in the thickness direction was applied in this nanocomposite system. The predicted real permittivity by VAM was found to be in better agreement with the measured data than that predicted by Bruggeman's equation.

Keywords: Magnetic; Ferroelectric; Nanostructures; Microwave properties

1. Introduction

Polymer nanocomposites have been reported for their potential wide applications such as UV shielding [1–4], electromagnetic interface shielding [5,6], microwave absorption [7,8] and stimuli–responsive structural biomimicking smart control [9] because of their easy processability, low-cost manufacturing and good adhesion to substrates. For microwave absorption, the fillers could be chosen from either magnetic or dielectric materials [10]. Most of the polymer matrices are insensitive to electromagnetic wave radiation and only serve as hosting binders between the nanoparticles. The hosting polymer chains facilitate local stress transfer from the polymer matrix to the tougher nanoparticles and provide good adhesion between the composite and the substrate. The active component of absorption is the magnetic or dielectric fillers, which absorb the microwave owing to the interactive loss process of dielectric or magnetic dipoles of the fillers [11]. Thus, composites with higher filler loading have great potential to increase absorption ability. However, subsequent manufacturing puts a limitation on the availability of high-quality nanocomposites with high filler loadings.

* Corresponding author. Current address: Chemical Engineering Department, Lamar University, Beaumont, TX 77710, USA. Tel.: +1 4098807654.
E-mail address: zhanhu.guo@lamar.edu (Z. Guo).

1359-6454/$34.00 © 2008 Acta Materialia Inc. Published by Elsevier Ltd. All rights reserved.
doi:10.1016/j.actamat.2008.09.024

High particle loading can cause heavy cracks or even bubbles (voids), which will definitely decrease the mechanical properties [12–14]. Towards achieving nanocomposites with high particle loading and good mechanical performance, coupling agents have been widely used to improve particle dispersion and to enhance the interaction between the nanoparticles and the polymer matrix [2,15,16].

Recently, a facile surface-initiated-polymerization (SIP) method has been introduced to fabricate polyurethane (PU) nanocomposites reinforced with single-phase iron oxide nanoparticles [17] or silicon carbide nanoparticles [18]. Both have shown improved mechanical properties in the composites with a high particle loading, and the filling materials are observed to have a significant effect on the mechanical behavior of the polymer. The superparamagnetic iron oxide nanoparticles were observed to behave as ferrimagnetic with increased coercivity (coercive force) due to the weaker dipolar interparticle interaction induced by the non-magnetic polymer spacer. Ferroelectric ceramics such as barium titanate possess a high dielectric constant with a great potential for energy storage supercapacitor [19] and dielectric microwave absorber applications [20–22]. The addition of two different types of nanoparticles could enhance the overall performance of the polymer nanocomposites by introducing individual constituent nanoparticles with different properties. However, there are few papers reporting on these.

In this paper, the SIP method is used to fabricate PU nanocomposites reinforced with two different nanoparticles, i.e., magnetic γ-Fe_2O_3 and ferrielectric barium titanate. The thermal stability of the nanocomposite was qualitatively characterized by thermogravimetric analysis (TGA), and the chemical interaction between nanoparticles and polymer was characterized by derivative thermogravimetry (DTG). The magnetic properties of the nanocomposites filled with different γ-Fe_2O_3 particle loadings and two different nanoparticles were investigated. The effect of high dielectric constant ceramic barium titanate nanoparticles and magnetic γ-Fe_2O_3 nanoparticles on the microwave properties (permittivity and permeability) of the PU nanocomposites was explored. The microwave properties were further analyzed by Bruggeman's equation and the volume average method (VAM). The feasibility of the VAM in microwave property prediction is discussed compared with the experimental measurement.

2. Experimental

2.1. Materials

The fillers used for composite fabrication are barium titanate powder ($BaTiO_3$, 50 nm, NanOxide™ HPB 1000, TPL, Inc., NM) and iron oxide (γ-Fe_2O_3, 23 nm, Nanophase Technologies Corporation) nanoparticles. The polymer matrix used was a commercial, clear PU coating (CAAPCOAT FP-002–55X, manufactured by the CAAP Co., Inc.). It contains two-part urethane monomers, i.e., 80 wt.% diisocyanate and 20 wt.% diol. The liquid resin has a density of 0.83 g cm^{-3}. The PU catalyst (a liquid containing ~20–65 wt.% aliphatic amine, 1–50 wt.% parachlorobenzotrifluoride and 10–35 wt.% methyl propyl ketone) and accelerator (PU STD-102, containing 1 wt.% organotitanate and 99 wt.% acetone) were provided by CAAP Co., Inc. All the chemicals were used as-received without further treatment.

2.2. Nanocomposite fabrication

The PU composites reinforced with magnetic (iron oxide) and/or ferroelectric (barium titanate) nanoparticles were fabricated by the recently developed SIP method [17,18]. SIP was observed to yield nanocomposites with a high particle loading up to 65 wt.% for iron oxide [17] and 35 wt.% for silicon carbide [18] in a PU matrix while still maintaining structural integrity. This method uses physicochemically adsorbed moisture and hydroxyl groups on the nanoparticles as a linking site between the nanoparticles and the polymer chains. The composite fabrication process is briefly described as follows. The nanoparticles were added into the catalyst–accelerator (CA) tetrahydrofuran (THF) solution and sonicated for ~1 h. The sonication energy enhances the reactivity of the surface and promotes the adsorption of CA onto the nanoparticle surface while evaporating the physically adsorbed moisture. The monomers were then introduced into the above solution dropwise within half an hour, and the polymerization was continued in the same conditions. The final solution was poured into a mold, and the solvent was evaporated naturally in ambient conditions.

2.3. Characterization

Particle structural characterization was performed by scanning electron microscopy (SEM; JEOL field emission scanning electron microscope, JSM-6700F).

The physicochemical attachment of the CA mixture onto the nanoparticle surface was verified by TGA (Perkin-Elmer). The sample was prepared by dispersing the nanoparticles into THF, adding the CA, stirring for half an hour, and washing the precipitated nanoparticles with excess THF to remove the extra CA. TGA was carried out from 25 to 600 °C with an argon flow rate of 50 cm^3 min^{-1} at a heating rate of 10 °C min^{-1}. Fourier transform infrared (FT-IR) spectrometry was used to characterize the CA on the nanoparticle surface further. Its spectra were recorded in a FT-IR spectrometer (Jasco, FT-IR 420) in transmission mode under dried nitrogen flow at 10 cm^3 min^{-1}. The FT-IR nanoparticle samples were prepared by mixing with powdered KBr, grinding and compressing into a pellet.

The thermal stability of the nanocomposites and the particle percentage in the nanocomposites were characterized and determined by TGA, following the same procedures as above. Particle dispersion in PU was

characterized by SEM. The SEM samples were prepared by embedding the nanocomposite in a cured vinyl-ester-resin tab and polishing the nanocomposite cross section. A thin gold coating was sputtered to improve the electric conductivity needed for high-quality SEM images.

The magnetic properties were investigated in a 9-Tesla Physical Properties Measurement System (PPMS) by Quantum Design.

The effective complex permittivity ($\varepsilon = \varepsilon' - j\varepsilon''$) and permeability ($\mu = \mu' - j\mu''$) of the polymer nanocomposites were measured using the transmission/reflection (TR) method based on the Nicolson–Ross algorithm [23–25], which is calculated from the measured scattering parameters (S parameters). The measurement was carried out with an Agilent E4991A impedance analyzer, combined with an Agilent 16453A dielectric material test fixture and an Agilent 16454A magnetic material test fixture, respectively, under a sweep of 10 MHz–1 GHz. Specimens for permittivity measurement were cylinders with diameter 17.5 mm, and those for permeability were hollow cylinders with inner diameter 10 mm and outer diameter 17.5 mm. The thickness of all the samples ranged from 0.5 to 2.0 mm.

3. Results and discussion

Fig. 1 shows the SEM microstructures of the as-received barium titanate (a–c) and iron oxide (d) nanoparticles. The $BaTiO_3$ nanoparticle sample was prepared by spreading the nanoparticles onto a double-sided carbon tape, which was fixed on an aluminum tab. The nanoparticles were observed to present as microparticles with smaller agglomerated nanoparticles. Except for the agglomerated small nanoparticles, discrete larger particles were observed without agglomeration. Similar phenomena were observed for the iron oxide nanoparticles, but, earlier TEM bright field examination [17] showed discrete nanoparticles after the nanoparticles were dispersed in ethanol and dropped onto a holey carbon-coated copper grid. This is due to the interparticle interaction difference with the presence of solvent. The ultrasonication during the TEM sample preparation is also responsible for the nanoparticle dispersion.

The TGA curves of the as-received nanoparticles depict continuous weight loss, as shown in Fig. 2, indicating the presence of either physically adsorbed moisture or chemically bonded hydroxyl groups and consistent with the formerly reported SiC and iron oxide nanoparticles [13,17]. Further TGA investigation justified physical adsorption of the CA mixture on the nanoparticle surface, shown in Fig. 2. The nanoparticle samples were prepared by adding nanoparticles into the CA THF solution with the aid of ultrasonication for activation of the nanoparticle surface. The CA–nanoparticle complex will serve as a catalyst unity for the subsequent monomer polymerization. The activated hydroxyl groups on the nanoparticle surface react with the subsequently added isocyanate, which further copolymerizes with urethane monomers (diol and isocyanate) for composite formation.

Fig. 3a shows the thermal stability of the PU nanocomposites fabricated by the SIP method. The nanocomposites are reinforced with iron oxide nanoparticles at different particle loadings. The decomposition of the nanocomposites was observed to begin ~240 °C and get full decomposition at temperatures >440 °C. The addition of the nanoparticles was observed to decrease the thermal stability of the nanocomposites, which is different from the alumina nanoparticle reinforced vinyl-ester-resin nanocomposites [15] and consistent with the zinc oxide nanoparticle reinforced vinyl-ester-resin nanocomposites [2]. This indicates that the nanofiller itself has a significant effect on the thermal stability of the polymer matrix. The thermal stability has little dependence on the particle loading at temperatures <240 °C and slightly decreases with the increase in nanoparticle loading at temperatures in the range 240–320 °C. The plateau at higher temperatures is due to the chemical redox reaction between the coked carbon and iron oxide. The final weight difference as shown in Fig. 3a is due to the different particle loadings.

Pure PU was found to have only one peak in the DTG curve, and the presence of the nanoparticles decreased the thermal stability of the PU matrix [17]. For the nanocomposite samples with a loading of 9.4 and 14.4 vol.%, three peaks were observed, as shown in Fig. 3b, reflecting the different interactions between the nanoparticles and the polymer matrix. In other words, the existence status of the polymer has a strong effect on the thermal stability of the polymer nanocomposites. However, a small peak between 350 and 400 °C is observed in the composite samples at lower loadings. The ratio of the peaks further indicates the amount of polymer on the nanoparticle surface and the bulk matrix. In the composite with higher particle loading, the ratio of the second peak to the first peak is much higher, indicating the dominating strong chemical interaction between the nanoparticles and the polymer matrix, which is in stark contrast to the weak physical interaction between the nanoparticle and the polymer matrix or freely existing polymer in the composites.

The effect of the nanofiller materials on the thermal stability was investigated. Fig. 4 shows the TGA and DTG curves of the PU nanocomposites reinforced with different particle loadings of $BaTiO_3$ nanoparticles. As compared with the larger plateau in the iron oxide nanoparticle reinforced PU nanocomposites, only a small bump in the temperature range 350–405 °C is observed in the nanocomposite with high particle loadings. Similar to that of the PU nanocomposites reinforced with iron oxide nanoparticles, the peak ratio difference at higher temperatures from that at lower temperatures observed in the nanocomposite reinforced with pure barium titanate nanoparticles indicates the different ratio of the polymer attached to the nanoparticle surface.

The synergistic effect of the iron oxide and $BaTiO_3$ nanoparticles on the thermal stability of the PU nanocomposites was investigated and compared with the single-phase nanoparticle reinforced PU nanocomposites. Here,

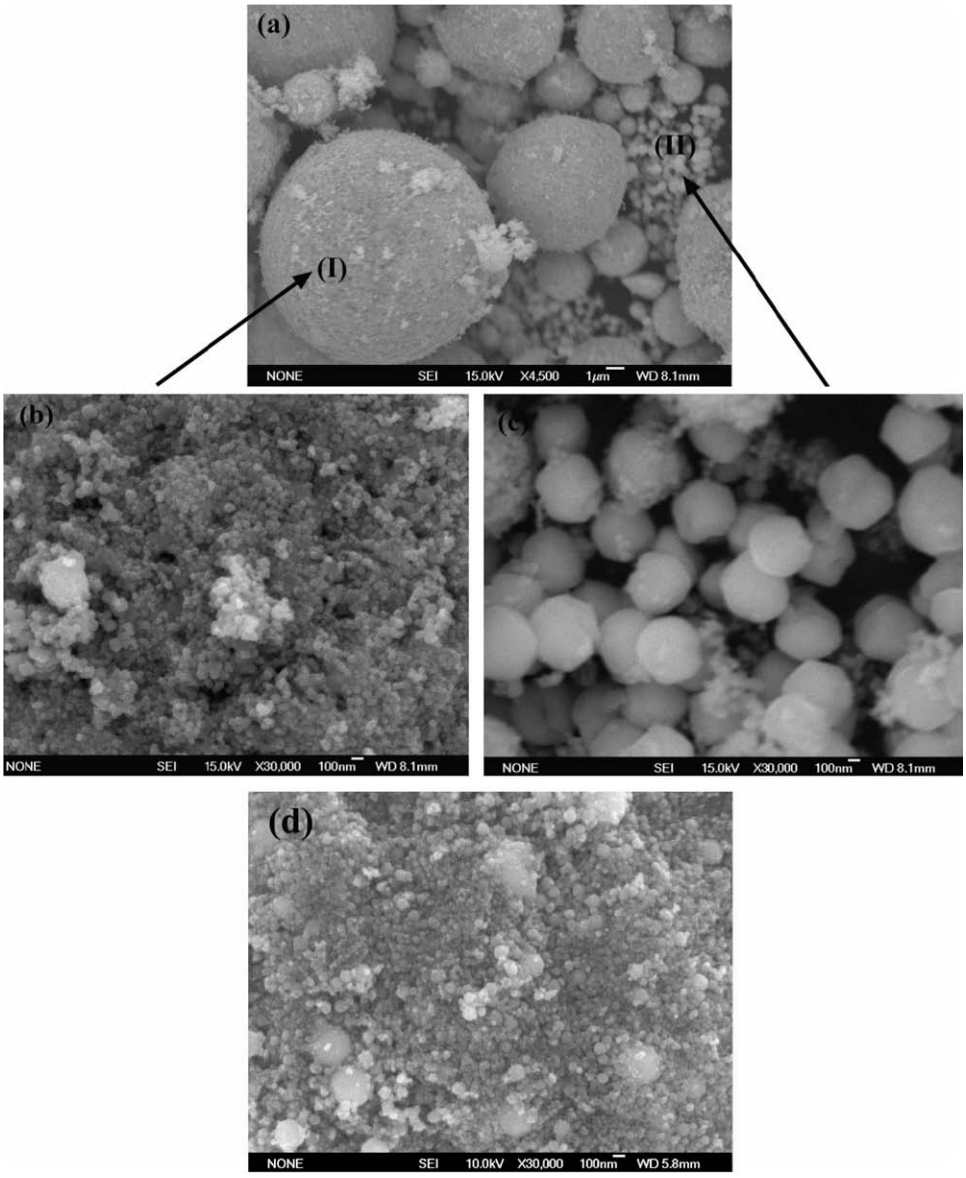

Fig. 1. SEM micrographs of as-received (a–c) barium titanate and (d) iron oxide nanoparticles; (b) and (c) represent the large and small barium titanate particles in (a).

only high particle loading with a different ratio of iron oxide and barium titanate nanoparticles was chosen. Fig. 5a shows the TGA curves of the PU nanocomposites reinforced with binary nanoparticles. The total particle loading is 60 wt.%, and the weight ratio of iron oxide to barium titanate is 2:8, 4:6 and 6:4, respectively. Little difference was observed at temperatures <330 °C. However, the plateau was obviously observed and increased with the increase in iron oxide particle loading. The TGA curve of the nanocomposite reinforced with a lower Fe_2O_3:$BaTiO_3$ (2:8 by weight) binary nanoparticle ratio is more similar to that of the nanocomposites reinforced with pure barium titanate particles. Conversely, the TGA curve of the nanocomposite with higher Fe_2O_3:$BaTiO_3$ (6:4 by weight) binary nanoparticle ratio is more similar to that of the nanocomposites reinforced with pure iron oxide nanoparticles. These phenomena indicate that the thermal decomposition of the nanocomposites reinforced with binary nanoparticles follows a simple physical mixing rule.

The particle distribution within the PU matrix was characterized by SEM. Former field emission SEM observation indicated uniformly dispersed iron oxide nanoparticles [17] and silicon carbide nanoparticles [18] in the PU matrix, even with a high particle loading. In order to obtain better mixing of the binary phase (iron oxide and barium titanate) nanoparticles, the biphasic nanoparticles were dispersed into THF under ultrasonication, and then the same SIP procedures were followed as for composite fabrication. No significant agglomeration was observed in the nanocomposite with a particle loading of 60 wt.% (Fe_2O_3:$BaTiO_3$ = 6:4 by weight), as shown in the typical SEM image in Fig. 6. This indicates that the SIP method is a fac-

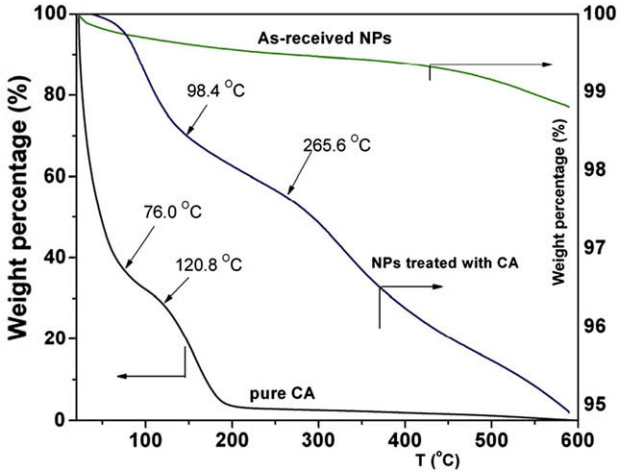

Fig. 2. TGA curves of the as-received $BaTiO_3$ nanoparticles, mixture of the CA and the CA-treated nanoparticles.

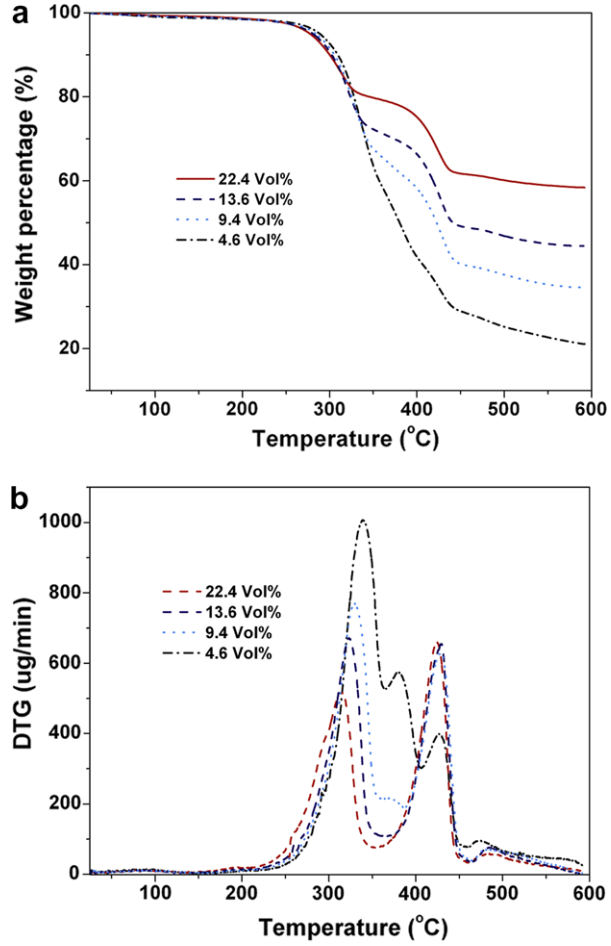

Fig. 3. (a) TGA and (b) DTG curves of the iron oxide nanoparticles reinforced PU nanocomposites with different particle loading.

ile and general method for fabricating high-quality nanocomposites reinforced with ceramic oxide nanoparticles.

The synergistic effect of the biphasic nanoparticles on the magnetic properties of the polymer nanocomposites was investigated. Fig. 7 shows the room temperature hys-

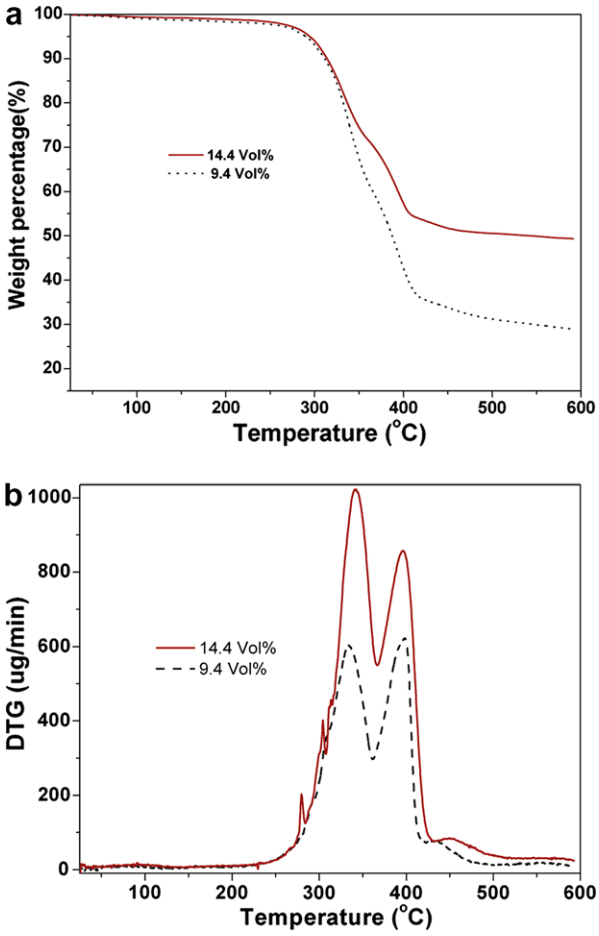

Fig. 4. (a) TGA and (b) DTG curves of the barium titanate nanoparticles reinforced PU nanocomposites with different particle loading.

teresis loop of the magnetic nanocomposites reinforced with pure iron oxide nanoparticles and binary (iron oxide and barium titanate) nanoparticles, respectively. The total particle loading is 60 wt.% for the binary nanoparticle system and different ratios of iron oxide to barium titanate. Coercivity (H_c, Oe) is an important physical parameter to distinguish a material whether it be hard (>100 Oe) or soft (<100 Oe). The coercivity is observed to be ~160 Oe in the polymer nanocomposites, as shown in the inset in Fig. 7, which is much larger than that (18 Oe) of the pure iron oxide nanoparticles [13]. In other words, the iron oxide nanoparticles were observed to become magnetically harder after dispersion in the polymer matrix. The saturation magnetization (M_s, emu g^{-1}) of the used iron oxide nanoparticles was measured to be 68 emu g^{-1} [13]. The M_s variation in the composites is due to the change in particle loadings. The magnetization of the composite is related to the weight percentage of the iron oxide nanoparticles rather than the volume percentage of the iron oxide. Furthermore, the addition of the dielectric barium titanate is observed to have little effect on the magnetic properties, which is due to the non-magnetic property of $BaTiO_3$.

Fig. 8a and b shows the microwave properties, i.e., real and imaginary permittivity and permeability of Fe_2O_3/PU

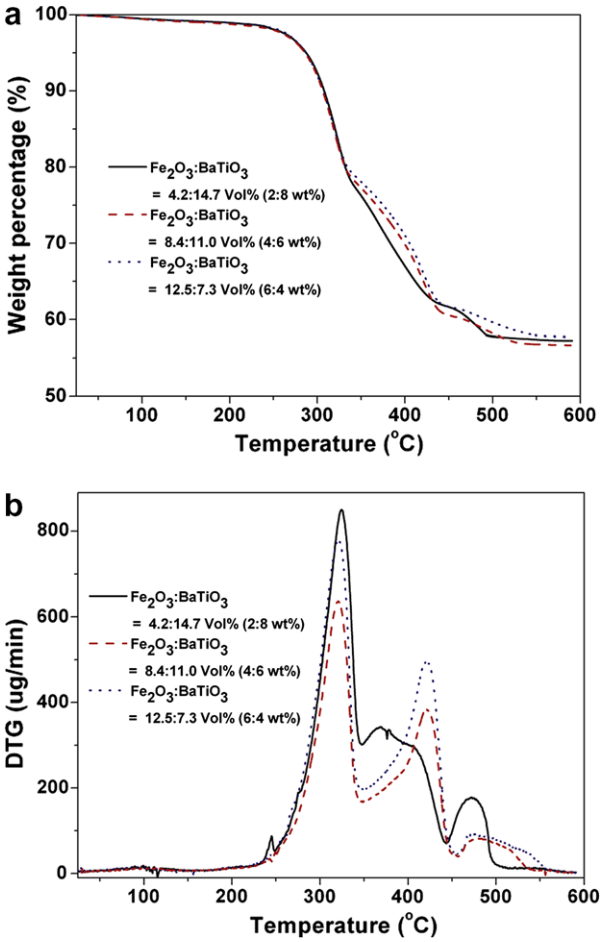

Fig. 5. (a) TGA and (b) DTG curves of the biphasic iron oxide and barium titanate nanoparticle reinforced PU nanocomposites at different ratios with a total particle loading of 60 wt.%.

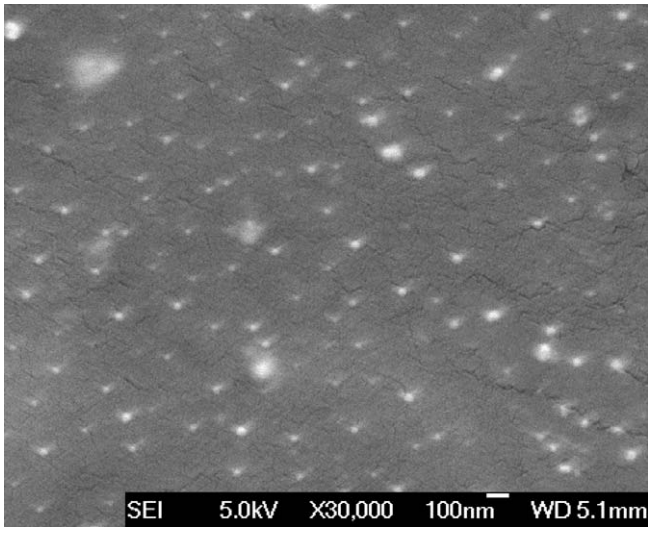

Fig. 6. SEM image of the PU nanocomposites reinforced with binary nanoparticles Fe_2O_3:$BaTiO_3$ (6:4 by weight).

nanocomposite, respectively. The real permittivity (or dielectric constant) of the composites was observed to increase with the decrease in frequency and was also observed to increase with the increase in particle loading. This tendency is consistent with other polymer nanocomposite systems such as epoxy [26] or polyaniline [27] nanocomposites loaded with γ-Fe_2O_3. The Fe_2O_3 nanoparticle reinforced PU nanocomposites were observed to have almost the same resonance frequency, ~500 MHz, as that (450 MHz) of the pure PU, as shown in Fig. 8a, which is due to the fact that iron oxide nanoparticles do not possess dielectric resonance in the frequency range of interest [26,28,29].

The permeabilities of Fe_2O_3/PU as shown in Fig. 8b were observed to be nearly constant in the low frequency range up to ~400 MHz and then to increase with the increase in frequency. This observed frequency-dependent permeability was consistent with that of Fe_2O_3/ZnO/epoxy nanocomposites in the megahertz and gigahertz ranges [26,30], considering the non-magnetic and dielectric properties of the ZnO nanoparticles, PU and epoxy. No magnetic resonance frequency was observed within the measured frequency range (up to 1 GHz). However, the drastic increase in imaginary permeability near 1 GHz is due to the magnetic resonance ~1 GHz and consistent with the Fe_2O_3/ZnO/epoxy composites with a reported resonance frequency near 1.5 GHz [26].

The permittivity of $BaTiO_3$/PU nanocomposites as shown in Fig. 9 was observed to be higher than that of the Fe_2O_3/PU nanocomposites with a similar particle loading at a given frequency. Similar to the Fe_2O_3/PU nanocomposites shown in Fig. 8b, the $BaTiO_3$/PU nanocomposites were observed to have a resonance frequency ~500 MHz).

The intrinsic microwave properties of the nanoparticles shown in Fig. 10 were calculated from the measured experimental data of the corresponding polymer nanocomposites and pure polymer matrix, as shown in Figs. 8 and 9 by the following Bruggeman's equation [26,31]:

$$\sum_{i=1}^{N}\left(V_i\frac{\varepsilon_i-\varepsilon_c}{\varepsilon_i+2\varepsilon_c}\right)=0 \quad (1)$$

where i denotes the constituent phases (filler(s) and PU), N is the number of constituent phases (2 for two phases and 3 for three phases), ε_i and V_i are the permittivity and volume fraction of ith phase, respectively, and ε_c is the measured permittivity of the polymer nanocomposites.

The intrinsic microwave properties of Fe_2O_3 and $BaTiO_3$ nanoparticles were reported to depend on the particle size, crystal structure, grain and its boundary condition, temperature and frequency [26,32–35]. However, there are few papers reporting on the intrinsic microwave properties of the nanoparticles, especially for frequency dependence. From the known volume fractions and the measured permittivities of polymer matrix and nanocomposites, the intrinsic properties of dispersed nanoparticles were calculated. This back-calculation approach can be used to investigate the size effect of the nanoparticles on

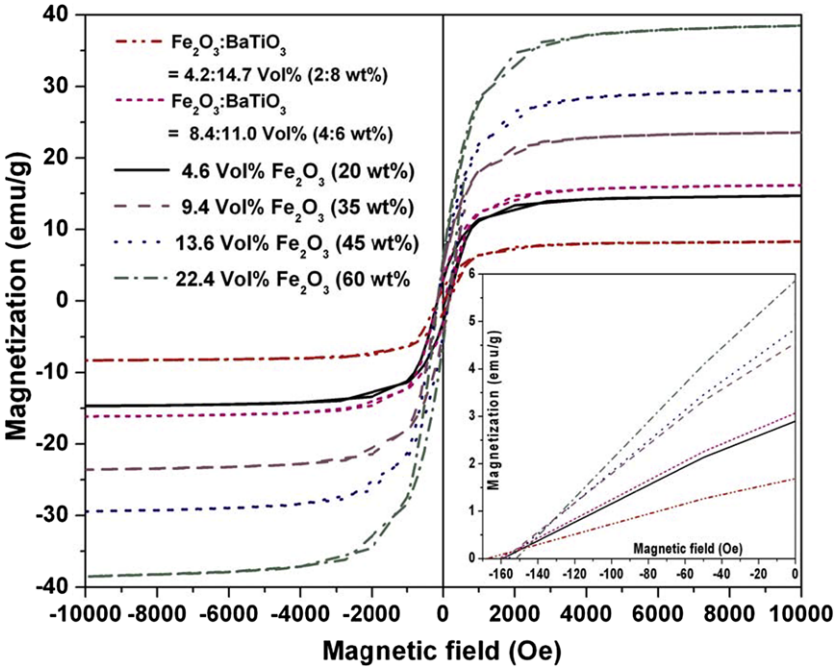

Fig. 7. Hysteresis loops of nanocomposites reinforced with 4.6 vol.% (20 wt.%), 9.4 vol.% (35 wt.%), 13.6 vol.% (45 wt.%) and 22.4 vol.% (60 wt.%) and binary nanoparticles (total weight percentage is 60 wt.%) (Fe_2O_3:$BaTiO_3$ = 2:8 and 4:6 by weight, respectively). Inset shows the enlarged hysteresis loop at low field.

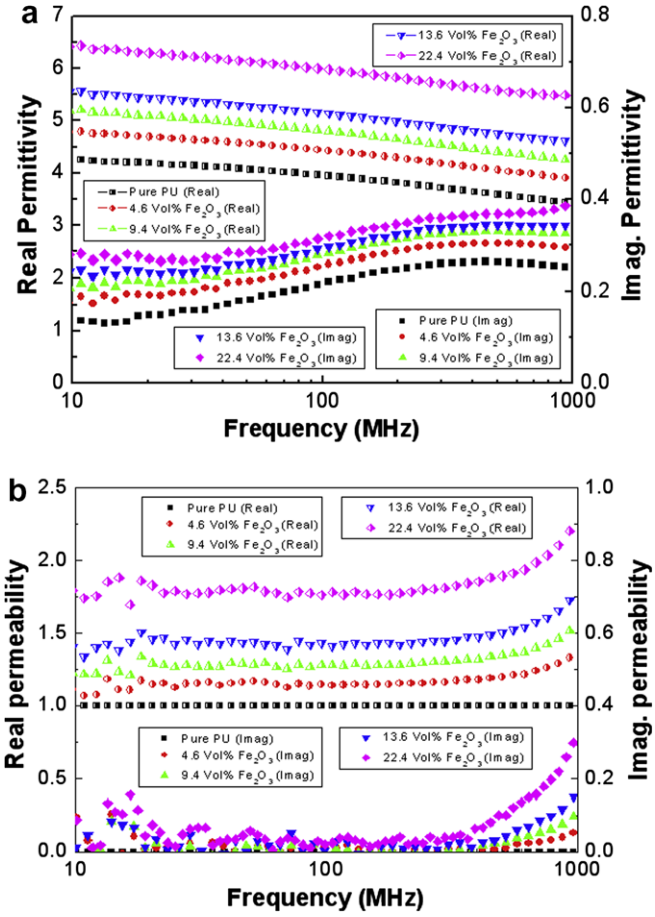

Fig. 8. (a) Permittivity and (b) permeability of Fe_2O_3/PU nanocomposites.

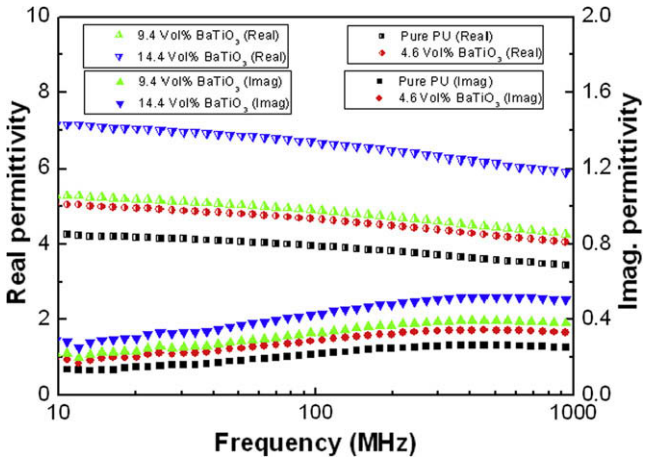

Fig. 9. Permittivity of $BaTiO_3$/PU nanocomposites.

the intrinsic microwave properties, which has also been successfully applied for polymer composites with micron- and nano-size dielectric or magnetic particles [28,29,32,36].

The intrinsic permittivity of Fe_2O_3 nanoparticles, as shown in Fig. 10a, was almost constant at ~22.0 in the whole measured frequency range, which is higher than the reported 14.2 at 1 GHz [26].

The permeability of Fe_2O_3 nanoparticles was ~10.0 at 100 MHz and then gradually increased and reached 30.0 at 1 GHz. The real permeability was back calculated by Lichtenecker's equation [29,37] and fell in the range 21–16 at a frequency 0.5–1 GHz [28,29]. The permeabilities were comparable with each other, even though the particle size was not mentioned in the studies [26,38] and could play

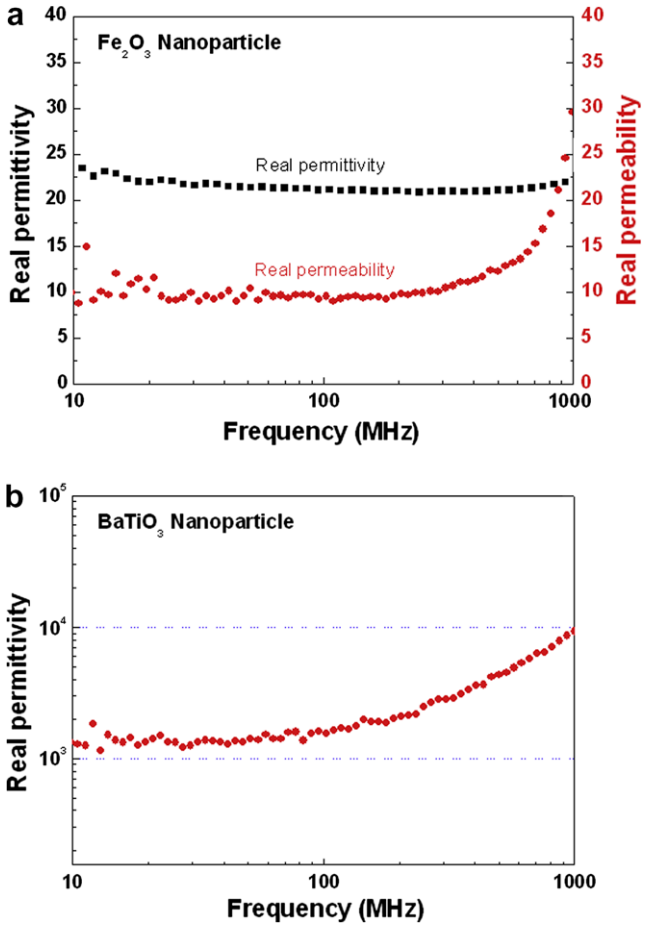

Fig. 10. (a) Intrinsic permittivity and permeability of Fe_2O_3 nanoparticles and (b) intrinsic permittivity of $BaTiO_3$ nanoparticles back calculated by Bruggeman's equation.

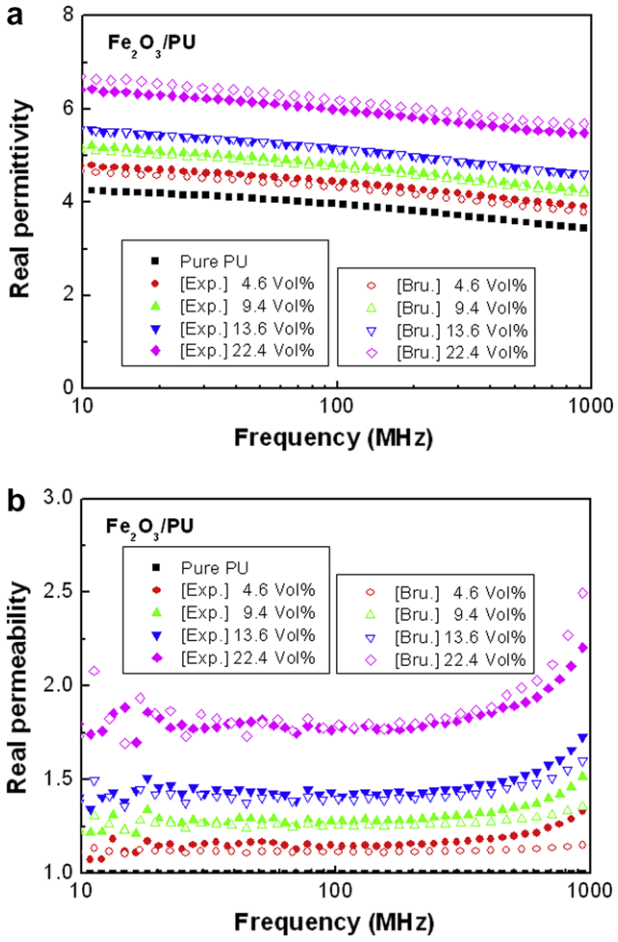

Fig. 11. Comparison between (a) measured real permittivities and (b) permeabilities of Fe_2O_3/PU nanocomposites with those predicted by Bruggeman's equation using back-calculated intrinsic properties of Fe_2O_3.

a critical role in the microwave performance, especially on a nano scale [26,38].

The permittivity of $BaTiO_3$ nanoparticles as shown in Fig. 10b was between 1100 and 1500 in the frequency range 10–100 MHz, comparable with the reported 1000 in other studies [32–35]. The permittivity was observed to increase gradually and reach almost 10,000 at 1 GHz. The dielectric constant of $BaTiO_3$ nanoparticles is reported to depend strongly on particle size and temperature, especially when the size is <300 nm, above which the property was almost constant [32–35]. However, no data report is available for the frequency-dependent permittivity of the $BaTiO_3$ nanoparticles.

Using the intrinsic properties in Figs. 9 and 10, the measured real permittivity and permeabilities of Fe_2O_3/PU and $BaTiO_3$/PU nanocomposites were fitted by Bruggeman's equation and are drawn in Figs. 11 and 12. The comparison showed that the measured properties agreed well with the predicted values.

The microwave properties of $Fe_2O_3/BaTiO_3$/PU nanocomposites, as shown in Fig. 13, were also measured in the frequency of interest in order to evaluate the synergetic effects of the two nanoparticles on microwave properties.

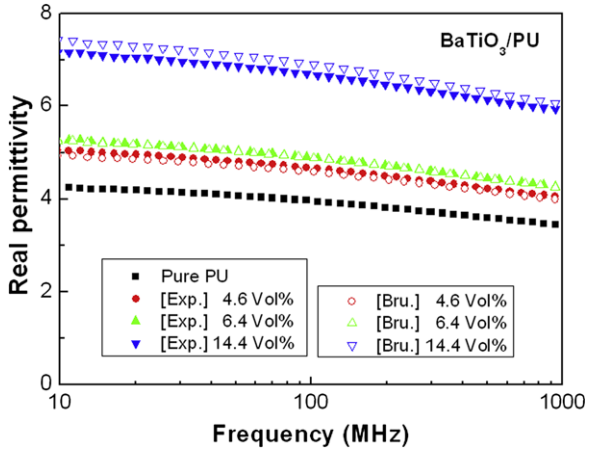

Fig. 12. Comparison between measured permittivities of $BaTiO_3$/PU nanocomposites with those predicted by Bruggeman equation using back-calculated intrinsic properties of Fe_2O_3.

Total particle weight per cent was kept at ~60 wt.%. The volume fractions of each particle of the binary nanoparticle composites were shown in Fig. 13. The real permittivity of the nanocomposites as shown in Fig. 13a was observed to

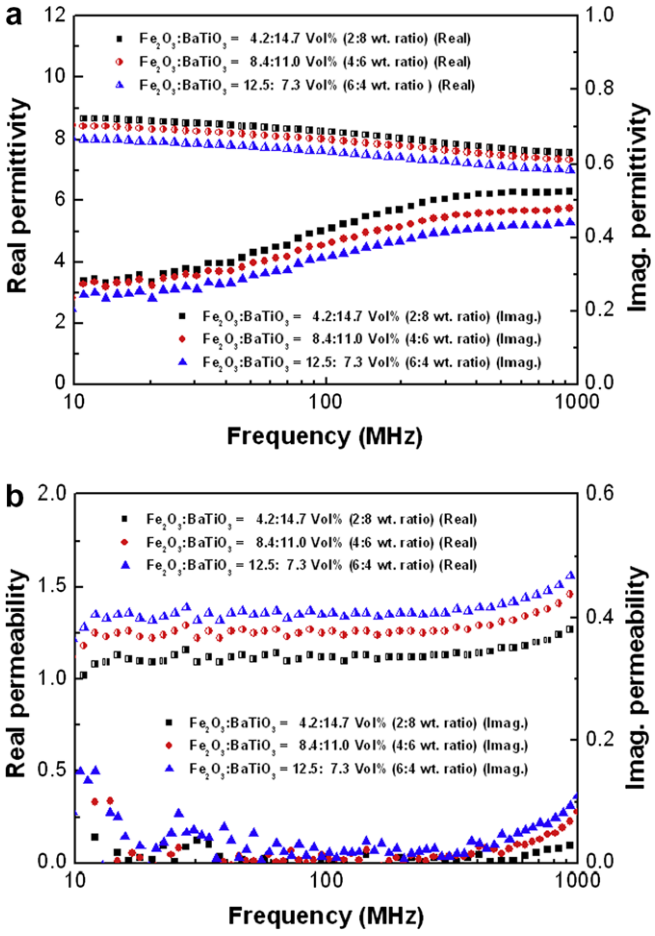

Fig. 13. (a) Permittivity and (b) permeability of $Fe_2O_3/BaTiO_3/PU$ nanocomposites according to particle loading ratio.

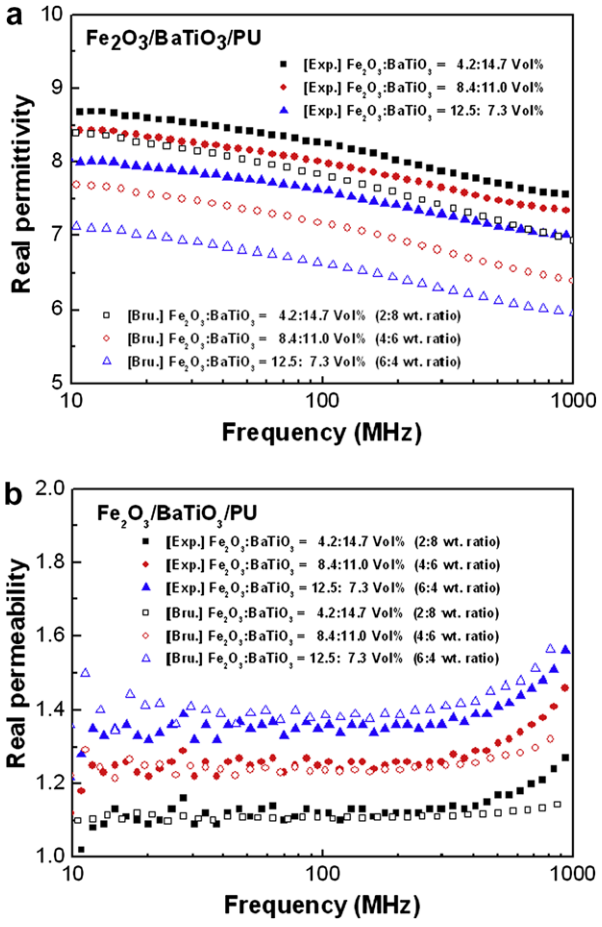

Fig. 14. Comparison between (a) measured real permittivities and (b) permeabilities of $Fe_2O_3/BaTiO_3/PU$ nanocomposites and those predicted by Bruggeman's equation.

increase with the decrease in Fe_2O_3 particle volume fraction. In other words, the real permittivity increases with increase in $BaTiO_3$ particle volume fraction. This is due to the higher ε_{BaTiO_3} than $\varepsilon_{Fe_2O_3}$, as shown in Fig. 10.

The permeability of the $Fe_2O_3/BaTiO_3/PU$ nanocomposites was observed to increase with the increase in Fe_2O_3 particle volume fraction, as shown in Fig. 13b. In addition, the permeability of Fe_2O_3/PU with 13.6 vol.% Fe_2O_3 particle loading shown in Fig. 11a is similar to that of $Fe_2O_3/BaTiO_3/PU$ with 12.5 vol.% Fe_2O_3 shown in Fig. 13b, indicating that permeability is dependent on the magnetic Fe_2O_3 only, rather than the non-magnetic $BaTiO_3$.

Fig. 14 shows the measured real permittivities and permeabilities of $Fe_2O_3/BaTiO_3/PU$ nanocomposites and those predicted by Bruggeman's equation, respectively. The measured permeability was found to be in a good agreement with the predicted permeability, as shown in Fig. 14b. The predicted permittivity was observed to decrease with the increase in frequency in the nanocomposites with different particle loadings. Furthermore, the predicted permittivity was found to decrease with the increase in Fe_2O_3 particle volume fraction. However, some deviation between the measured and predicted permittivities is observed, as shown in Fig. 14a, which could be due to the interfacial polarization effect [39].

A VAM was used to predict the effective mechanical and thermal properties of multidirectional fiber-reinforced composites which have reinforcements in out-of-plane directions [37]. The model takes into consideration an unequal volumetric distribution of reinforcements in different directions and is consistent with an existing analytical model based on the laminate theory and with experimental results [40,41] The VAM method can be mathematically expressed in Eq. (2):

$$[\varepsilon_c] = \sum_{i=1}^{2} \frac{V_{f_i}}{V_f} [T]_i^T [\varepsilon_c'']_i [T]_i \tag{2}$$

where V_{f_i} is the volume fraction of ith phases or fillers, $V_f = \sum_{i=1}^{2} V_{f_i} = V_{Fe_2O_3} + V_{BaTiO_3}$, $[T]_i$ is the transformation matrix from a local coordinate system to a global one, matrix $[\varepsilon_c]$ denotes the effective permittivity of the whole composites, and matrix ε_{ci}'' means permittivity of a composite with ith phase as a filler in the local coordinate system [37]. In this study, the coordinate transformation matrix is assumed to be a unit matrix with an assumption that all the particles are spherical and randomly distributed

within the polymer matrix. Therefore, the permittivity matrix is calculated from the total volume fraction and then weighed by volume fraction of the *i*th phase over the total filler volume fraction. Eq. (2) can be re-expressed:

$$\varepsilon_c = \frac{V_{Fe_2O_3}}{V_{Fe_2O_3} + V_{BaTiO_3}} \varepsilon_{c,Fe_2O_3} + \frac{V_{Fe_2O_3}}{V_{Fe_2O_3} + V_{BaTiO_3}} \varepsilon_{c,BaTiO_3} \quad (3)$$

ε_{c,Fe_2O_3} and $\varepsilon_{c,BaTiO_3}$ denote the effective permittivity of nanocomposites with Fe_2O_3 and $BaTiO_3$ only, and they are calculated in the volume fraction of $V_f = V_{Fe_2O_3} + V_{BaTiO_3}$. Eq. (3) can also be employed to predict the effective permeabilities. Fig. 15 shows the comparison between the measured real permittivities of Fe_2O_3/$BaTiO_3$/PU nanocomposites and those predicted by VAM. The predicted results agree well with the measured data and are much better than those predicted from Bruggeman's equation, as shown in Fig. 14. In addition, the permeability of composites predicted by VAM was also consistent with the measured permeability. Therefore, it can be concluded that the VAM can also be employed to predict the microwave properties of the binary particle nanocomposites.

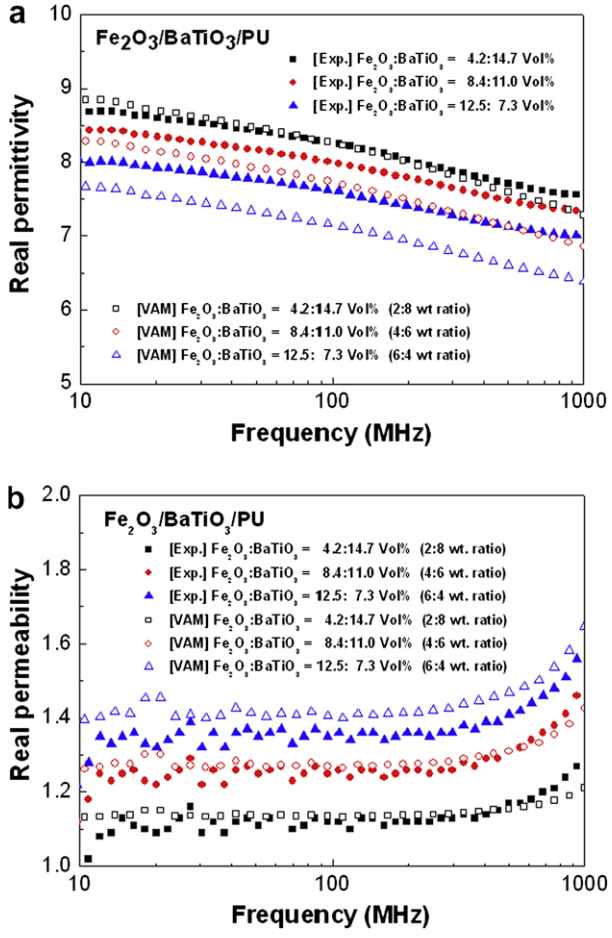

Fig. 15. Comparison between (a) measured real permittivities and (b) permeabilities of Fe_2O_3/$BaTiO_3$/PU nanocomposites and those predicted by VAM.

4. Conclusion

Polyurethane nanocomposites reinforced with two different nanoparticles, i.e., magnetic γ-Fe_2O_3 and ferroelectric barium titanate nanoparticles, were successfully prepared by the SIP method. The catalyst and accelerator nanoparticle complex as suggested by the TGA investigation favors chemical bond formation between the nanoparticles and the PU matrix, which is responsible for the subsequent SEM observed uniform particle dispersion in the matrix. The investigation on the thermal stability and the chemical interaction between nanoparticles and polymer indicated a synergistic effect of the biphasic nanoparticles on the polymer matrix. Different ratios of the polymer physically or chemically interacted with the particles, as indicated by the DTG analysis. Little magnetic change was observed after the ferroelectric $BaTiO_3$ nanoparticles were added into PU nanocomposites reinforced with magnetic iron oxide nanoparticles. The microwave properties of the nanocomposites were dependent on the frequency range and particle loadings. The intrinsic microwave properties of the nanoparticles were calculated from the measured data of the polymer nanocomposites and the pure polymer matrix. The real permittivity increased with the increase in particle loading. The addition of $BaTiO_3$ has little effect on the permeability of the biphasic nanoparticle reinforced PU nanocomposites.

Bruggeman's equation was introduced to evaluate the microwave properties of the nanocomposites and to investigate the intrinsic properties of the nanoparticles. The equation successfully predicted the microwave properties of nanocomposites reinforced with only one-phase and two-phase nanoparticles, except for the real permittivity of Fe_2O_3/$BaTiO_3$/PU. The effective permittivity and permeability predicated by the newly introduced VAM showed a more reasonable agreement with the measured data than that predicted by Bruggeman's equation. This indicates that the VAM method can be used effectively for calculating the microwave properties of nanocomposites with multiphases.

Acknowledgements

This work was financially supported by Northrop Grumman Corporation, with Dr. Sung Park as the program manager. Z. Guo appreciates the partial support from the UC-Discovery Grant ELE06-10268 and QuantumSphere Research Grant (QuantumSphere Inc.). D.P.Y. gratefully acknowledges support from the National Science Foundation under Grant No. DMR 04-49022.

References

[1] Sun D, Miyatake Ni, Sue H-J. Nanotechnology 2007;18:215606.

[2] Guo Z, Wei S, Shedd B, Scaffaro R, Pereira T, Hahn HT. J Mater Chem 2007;17:806.
[3] Zhang D, Downing JA, Knorr FJ, McHale JL. J Phys Chem B 2006;110:21890.
[4] Li Y-Q, Fu S-Y, Yang Y, Mai Y-W. Chem Mater 2008;20:2637.
[5] Zhang S, Ni Q, Fu Y, Kurashiki K. Compos Sci Technol 2007;67:2973.
[6] Gass J, Poddar P, Almand J, Srinath S, Srikanth H. Adv Funct Mater 2006;16:71.
[7] Bregar VB. IEEE Trans Magn 2004;40:1679.
[8] Guo Z, Park S, Hahn HT, Wei S, Moldovan M, Karki AB, et al. J Appl Phys 2007;101:09M511.
[9] Capadona JR, Shanmuganathan K, Tyler DJ, Rowan SJ, Weder C. Science 2008;39:1370.
[10] Zhang XF, Dong XL, Huang H, Liu YY, Wang WN, Zhu XG, et al. Appl Phys Lett 2006;89:053115.
[11] Abbas SM, Dixit AK, Chatterjee R, Goel TC. Mater Sci Eng B 2005;123:167.
[12] Zhang X, Simon LC. Macromol Mater Eng 2005;290:573.
[13] Guo Z, Lei K, Li Y, Ng H, Hahn HT. Compos Sci Technol 2008;68:1513.
[14] Rodgers RM, Mahfuz H, Rangari VK, Chisholm N, Jeelani S. Macromol Mater Eng 2005;290:423.
[15] Guo Z, Pereira T, Choi O, Wang Y, Hahn HT. J Mater Chem 2006;16:2800.
[16] Guo Z, Liang X, Pereira T, Scaffaro R, Hahn HT. Compos Sci Technol 2007;67:2036.
[17] Guo Z, Park S, Wei S, Pereira T, Moldovan M, Karki AB, et al. Nanotechnology 2007;18:335704.
[18] Guo Z, Kim TY, Lei K, Pereira T, Sugar JG, Hahn HT. Compos Sci Technol 2008;68:164.
[19] Burn I, Smyth DM. J Mater Sci 1972;7:339.
[20] McNeal MP, Jang S-J, Newnham RE. J Appl Phys 1998;83:3288.
[21] Dhage SR, Pasricha R, Ravi V. Mater Lett 2005;59:1053.
[22] Pant HC, Patra MK, Verma A, Vadera SR, Kuamr N. Acta Mater 2006;54:3163.
[23] Nicolson AM, Ross GF. IEEE Trans Instrum Meas 1970;IM-19:377.
[24] Nicolson AM. IEEE Trans Instrum Meas 1968;17:395.
[25] Brosseau C, Talbot P. IEEE Trans Dielectr Electr Insul 2004;11:819.
[26] Brosseau C, Youssef JB, Talbot P, Konn A-M. J Appl Phys 2003;93:9243.
[27] Mallikarjuna NN, Manohar SK, Klkarni PV, Venkataraman A, Aminabhavi TM. J Appl Polym Sci 2005;97:1868.
[28] Birks JB. Nature 1947;159:775.
[29] Crouch JGE, Willis CH. Ferromagnetic resonance in iron oxides. Report 13B, Princeton University, Princeton, NJ; 1949.
[30] Brosseau C, Mellegol S, Queffelec P, Youssef JB. Phys Rev B 2004;70:092401.
[31] Sihvola, A. Electromagnetic mixing formulas and applications (Institution of Electrical Engineers), Stevenage; 1999.
[32] Wada S, Hoshina T, Yasuno H, Nam SM, Kakemoto H, Tsurumi T, et al. J Korean Phys Soc 2005;46:303.
[33] Zhao Z, Buscaglia V, Viviani M, Buscaglia MT, Mitoseriu L, Testino A, et al. Phys Rev B 2004;70:024107.
[34] Wada S, Hoshina T, Yasuno H, Ohishi M, Kakemoto H, Tsurumi T, Yashima M. Seramikkusu Kiso Kagaku Toronkai Koen Yoshishu 2005;89.
[35] Ohno T, Suzuki D, Suzuki H, Ida T. KONA 2004;22:195.
[36] Wu M, Zhang H, Yao X, Zhang L. J Phys D Appl Phys 2001;34:889.
[37] Yoo JS, Lee SE, Kim CG. Compos Struct 2001;54:57.
[38] Cullity BD. Introduction to magnetic materials. Reading (MA): Addison-Wesley; 1972.
[39] Hallouet B, Wetzel B, Pelster R. J Nanomater 2007:34527.
[40] Mukherjee N, Sinha PK. Comput Struct 1997;65:809.
[41] Mukherjee N, Sinha PK. Compos Struct 1994;28:333.